



OPEN

Selective ^{13}C labelling reveals the electronic structure of flavocoenzyme radicals

Erik Schleicher¹✉, Stephan Rein¹, Boris Illarionov², Ariane Lehmann¹, Tarek Al Said¹, Sylwia Kacprzak^{1,5}, Robert Bittl³, Adelbert Bacher⁴, Markus Fischer² & Stefan Weber¹✉

Flavocoenzymes are nearly ubiquitous cofactors that are involved in the catalysis and regulation of a wide range of biological processes including some light-induced ones, such as the photolyase-mediated DNA repair, magnetoreception of migratory birds, and the blue-light driven phototropism in plants. One of the factors that enable versatile flavin-coenzyme biochemistry and biophysics is the fine-tuning of the cofactor's frontier orbital by interactions with the protein environment. Probing the singly-occupied molecular orbital (SOMO) of the intermediate radical state of flavins is therefore a prerequisite for a thorough understanding of the diverse functions of the flavoprotein family. This may be ultimately achieved by unravelling the hyperfine structure of a flavin by electron paramagnetic resonance. In this contribution we present a rigorous approach to obtaining a hyperfine map of the flavin's chromophoric 7,8-dimethyl isoalloxazine unit at an as yet unprecedented level of resolution and accuracy. We combine powerful high-microwave-frequency/high-magnetic-field electron–nuclear double resonance (ENDOR) with ^{13}C isotopologue editing as well as spectral simulations and density functional theory calculations to measure and analyse ^{13}C hyperfine couplings of the flavin cofactor in DNA photolyase. Our data will provide the basis for electronic structure considerations for a number of flavin radical intermediates occurring in blue-light photoreceptor proteins.

Amino acids surrounding an enzymatic cofactor alter its chemical reactivity by providing an environment required to bind and act upon a specific substrate and by adjusting the electronic properties of the cofactor through weak interactions including hydrogen bonding, dipolar couplings, and π -stacking. To quantify the parameters that modulate the catalytic power of an enzyme is one of the most fundamental challenges in modern biochemistry and biophysics. In this context, proteins with flavin cofactors are of particular interest because their functions are widespread: Since their discovery in the 1930s¹ flavins (see Fig. 1A) have been recognized as nearly ubiquitous cofactors that are involved in the catalysis of a wide range of biological redox processes^{2,3}. They serve as electron transmitters in electron-transfer processes such as oxidative phosphorylation⁴. Furthermore, flavins can act as mediators between typical two-electron donors such as NADH and one-electron acceptors such as the heme group. The ability of flavins to engage in one- as well as in two-electron-transfer reactions is due to their inherent property of adopting three different redox states^{5,6}. Besides their involvement in redox reactions, flavins also catalyse reactions without a net redox change such as blue-light sensing and the repair of UV-light-induced DNA lesions^{7–11}. In these processes, the metastable one-electron reduced radical form plays an essential role, either as a reaction intermediate¹² or, in case of receptor functioning, as a putative signalling state^{13,14}.

Starting in the early 1980s, considerable effort was invested in solving the puzzle of how flavin cofactors are modulated to optimize their properties for the catalysis of a specific reaction¹⁵. Artificially altered flavins, such as 8-azidoflavin or 5-deazaflavin, were incorporated into various proteins to replace the native cofactor. This strategy has been proven quite valuable, since cofactor analogues with, e.g. chemically reactive substituents can be used as probes of the flavin environment. However, artificial flavins exhibit different redox potentials, chemical properties and reactivity, and consequently, modify catalytic rates¹⁶. Therefore, for the study of the specific

¹Institut für Physikalische Chemie, Albert-Ludwigs-Universität Freiburg, Albertstr. 21, 79104 Freiburg, Germany. ²Institut für Lebensmittelchemie, Universität Hamburg, Grindelallee 117, 20146 Hamburg, Germany. ³Fachbereich Physik, Freie Universität Berlin, Arnimallee 14, 14195 Berlin, Germany. ⁴Department Chemie, Technische Universität München, Lichtenbergstr. 4, 85748 Garching, Germany. ⁵Present address: Bruker BioSpin GmbH, Silberstreifen 4, 76287 Rheinstetten, Germany. ✉email: erik.schleicher@pc.uni-freiburg.de; stefan.weber@pc.uni-freiburg.de

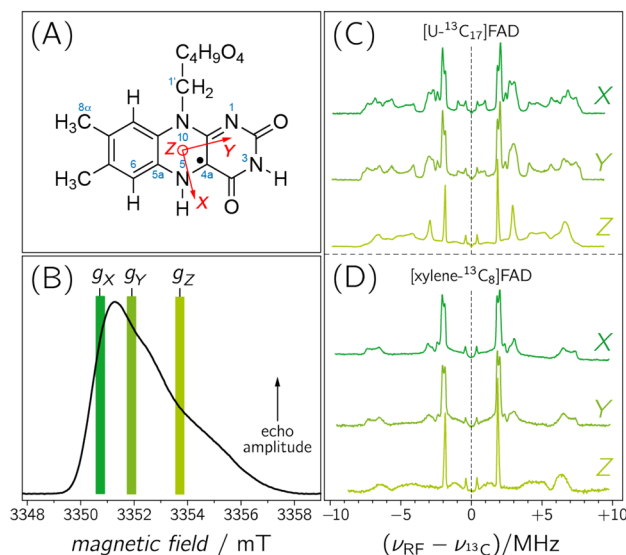


Figure 1. (A) IUPAC numbering of riboflavin (including the principal axes of the g -matrix). (B) Pulsed EPR spectrum of photolyase recorded with a microwave frequency of 94.0 GHz at a temperature of 80 K. The magnetic-field positions of the three principal values of the g -matrix ($g_x = 2.00429(2)$, $g_y = 2.00359(2)$, and $g_z = 2.00218(2)$), at which ENDOR spectra were recorded (dark green at g_x , medium green at g_y and light green at g_z , respectively), were taken from the literature. (C) and (D): Frozen-solution Davies-type ENDOR spectra of photolyase reconstituted with $[U-^{13}C_{17}]FAD$ (C) and $[xylene-^{13}C_8]FAD$ (D).

electronic structure of natural flavin cofactors in a variety of protein environments, a more sensitive and less intrusive method is required, e.g. based on isotope labelling of the cofactor and/or the protein^{17,18}.

The most sensitive and accessible probes of the electronic structure of a cofactor in its paramagnetic state are the electron Zeeman interaction and electron–nuclear hyperfine couplings (hfc). The isotropic contributions of the latter reflect the unpaired electron spin density at the positions of magnetic nuclei ($|A_{iso}| \sim |\Psi(0)|^2$)¹⁹. In most cases, these parameters can be precisely measured using electron paramagnetic resonance (EPR) and/or electron–nuclear double resonance (ENDOR). Up to now, however, mostly proton hfc from different flavoproteins have been exploited for this purpose^{20–24}. Unfortunately, hfc of protons are insufficient to draw a precise picture of the electron-spin density distribution in flavins as most protons are relatively remote from locations of high unpaired electron-spin density in the π -system of the 7,8-dimethyl isoalloxazine moiety, and furthermore, because protons in flavins are relatively scarce. Mapping the unpaired electron-spin density by directly measuring ^{13}C hfc using ENDOR is much more promising, but has been hampered by (i) the low natural abundance of ^{13}C , (ii) the limited availability of ^{13}C flavin isotopologues, and (iii) the strong overlap of ^{13}C hyperfine resonances with those arising from other magnetic nuclei, predominantly nitrogens, in ENDOR spectra recorded with EPR frequencies around 10 GHz, so that an unambiguous signal assignment could not be achieved.

In this contribution we exploit the potential of high-field ENDOR^{25–28} in combination with selective isotopologue editing to overcome the problem of measuring and assigning ^{13}C hfc of a flavin cofactor in its native protein environment. This facilitates a thorough mapping of the hyperfine structure and hence will ultimately allow theoreticians to draw quantitative conclusions on unpaired electron spin densities of flavocoenzymes in their functional surroundings. The ENDOR signals of ^{13}C nuclei are disentangled from resonances of other magnetic nuclei, such as 1H and $^{14/15}N$, at very high magnetic fields where the Larmor frequencies become increasingly different. Under such conditions, the ^{13}C hfc can be analysed uncompromised by spectral overlap. Furthermore, pulsed ENDOR performed at magnetic fields where the g -matrix anisotropy of a radical becomes dominant provides improved spectral resolution enabling the selection of molecules with specific orientations with respect to the direction of the external magnetic field even in a non-oriented sample^{29,30}. Due to the small g -matrix anisotropy typically observed in flavins^{31,32}, experiments performed at high magnetic field, high microwave and radio frequencies are expected to provide increased orientation selection effects that allow to evaluate the extent of hyperfine anisotropy.

To obtain unequivocal assignments of the ^{13}C ENDOR signals to individual carbons in the 7,8-dimethyl isoalloxazine moiety of the flavin, we recorded pulsed ENDOR spectra at W-band EPR frequencies of a flavoprotein, which had been produced with a variety of flavin isotopologues carrying ^{13}C atoms at strategic positions. The flavin adenine dinucleotide (FAD) binding DNA photolyase from *Escherichia coli* was chosen as a paradigm system for a proof of concept for several reasons: (i) The established purification procedure directly affords the neutral semiquinone radical, FADH \cdot ; (ii) the paramagnetic flavin form is a reactive intermediate in the enzymatic DNA-repair cycle of the protein³³; (iii) high-resolution structure data are available from X-ray crystallography^{34,35}; and (iv) flavin radicals in the photolyase/cryptochrome protein family have been proposed as key factors in some animal magnetoreception mechanisms that are believed to be based on correlated radical-pair spin chemistry^{13,36,37}.

Results and discussion

The frozen-solution echo-detected EPR signal of FADH^{*} in *E. coli* DNA photolyase recorded with a microwave frequency of 94.0 GHz is shown in Fig. 1B. The radical signature is clearly asymmetric because the electron-Zeeman anisotropy, determined by the **g**-matrix of FADH^{*}, exceeds the inhomogeneous spectral linewidth. By recording ENDOR spectra at different magnetic field positions in the resonance range one can now detect molecules with particular orientations with respect to the direction of the external magnetic field vector **B**₀^{29,38,39}. For example, recording ENDOR at a magnetic-field strength *B*₀ corresponding to the principal value *g*_Z of FADH^{*} reveals hyperfine data of those molecules whose principal **Z** axis is aligned parallel to **B**₀ thus resembling data from a partially oriented sample. The situation is slightly more intricate at *g*_Y, or in case of a **g**-matrix anisotropy approaching axial symmetry (i.e. *g*_X ≈ *g*_Y) also at *g*_X: the resulting ENDOR spectra become less “pure” and comprise resonances from molecules within a range of orientations predominantly with respect to the **g** principal axes **X** and **Y**. The extent of hyperfine anisotropy and the directions of the principal axes of the hyperfine matrix with respect to those of the **g**-matrix can still be analysed using spectral simulations.

Accordingly, Fig. 1C shows Davies-type pulsed ENDOR data of photolyase produced with uniformly ¹³C-labeled FAD ([U-¹³C₁₇]FAD) and recorded at different magnetic field strengths *B*₀. Within the weak-hfc limit (i.e. |hfc| ≪ *v*_{13C}), numerous pairs of hyperfine resonances are observed that are symmetrically arranged around the free ¹³C-Larmor frequency *v*_{13C}. The spectra recorded at the three canonical orientations of the **g**-matrix, i.e. at *g*_X, *g*_Y and *g*_Z, are clearly distinct due to the above-mentioned orientation-selection effects. In sets of such spectra, hfc components of a specific ¹³C nucleus can now be directly extracted from the splittings between associated hyperfine resonances with the aid of spectral simulations (see Supplementary Information).

Despite the additional information from the anisotropy of the hfcs, the resonances arising from 17 ¹³C-hfcs in [U-¹³C₁₇]FAD are not readily assigned. To disentangle the rather complex ENDOR spectra of the [U-¹³C₁₇]FAD-labelled photolyase, application of selective isotope editing is an obvious requirement. Figure 1D shows ENDOR spectra of the protein reconstituted with [5a,6,7,7a,8,8a,9,9a-¹³C₈]FAD ([xylene-¹³C₈]FAD), recorded under the same experimental conditions. As expected, fewer signals are now observed, and by employing quantum-chemical computations of ¹³C hfcs, one could envisage an assignment provided that the theoretical predictions are sufficiently precise. However, the reliability of hyperfine predictions strongly depends on the structural model used, and only in very rare cases do calculated and experimental hfcs of more complex aromatic cofactors, such as flavins, agree to within ± 15% or less^{40,41}. Consequently, to achieve an unambiguous assignment of hyperfine resonances, examinations of isotopologues with even fewer ¹³C atoms are desirable. Therefore, a library of FAD isotopologues with two or three strategically positioned ¹³C atoms has been devised and examined by high-magnetic-field/high-microwave-frequency ENDOR.

As expected, limitation to fewer ¹³C nuclei per sample considerably simplifies ENDOR spectra; Fig. 2 depicts sets of spectra of photolyase reconstituted with various [¹³C]FAD isotopologues: [6,8α-¹³C₂]FAD (panel A), [5a,8-¹³C₂]FAD (panel B), [1',7α,9-¹³C₃]FAD (panel C), [2,4a-¹³C₂]FAD (panel D), and [4,10a-¹³C₂]FAD (panel E). Hyperfine resonances are now sufficiently sparse and well separated such that with the help of (i) a global fit strategy with sophisticated parameter sampling for spectral simulations, (ii) quantum-chemical calculations, (iii) orientation selection of the hyperfine matrix, and (iv) calculations of difference spectra to reduce the complexity of the ENDOR data, a nearly complete hyperfine mapping of all carbons in the isoalloxazine moiety of the flavin can be achieved.

Specifically, ENDOR data at three different magnetic field positions corresponding to *g*_X, *g*_Y and *g*_Z were collected for each isotopologue (see Fig. 2). As the principal axes of a hyperfine matrix are determined by the specific bonding situation of the atom, the projection values of the hyperfine matrix (*A*_X, *A*_Y, *A*_Z) can now be extracted with respect to the principal axes (**X**, **Y**, **Z**) of the **g**-matrix on the basis of spectral simulations of the ENDOR data. In some equivocal cases, and for obtaining the signs of hfcs, our analysis was aided by quantum-chemical computations. We used density functional theory (DFT) at the B3LYP/EPR-II level of theory to calculate ¹³C-hfcs of the isoalloxazine chromophore bound to photolyase based on the three-dimensional coordinates of the enzyme from X-ray crystallography³⁴. Detailed descriptions of signal assignments can be found in the Supplementary Information (Figs. S1 to S5 and Tables S1 to S5). The sets of hyperfine projections arising from C7 and C9a were obtained using difference-ENDOR spectroscopy. For this purpose, the respective orientation-selective ENDOR spectra of photolyases reconstructed with [5a,8-¹³C₂]FAD, [6,8α-¹³C₂]FAD and [1',7α,9-¹³C₃]FAD were subtracted from those with [xylene-¹³C₈]FAD as cofactor to obtain ENDOR data of the fictitious [1',7,9a-¹³C₃]FAD-containing photolyase (see Fig. S6 and Table S6).

Only the *A*_Z component of C4a could not be determined by the present strategy: DFT calculations predict very strong anisotropy for the C4a hyperfine matrix, and for its *A*_Z component values exceeding + 50 MHz. Such strong anisotropy is conducive to spreading signal intensity over a wide radio frequency range, and hence, results in low absolute signal amplitude. Therefore, only two out of the three hyperfine components could be directly measured by ENDOR. We have also applied other pulsed hyperfine methods (such as electron-spin-echo envelope modulation and hyperfine-sublevel correlation at X-band) to detect *A*_Z(C4a) of a neutral flavin radical, but did not obtain unambiguous results.

Finally, the hyperfine projections, *A*_X, *A*_Y, and *A*_Z were averaged to obtain the isotropic hfc of a particular ¹³C nucleus: *A*_{iso} = (*A*_X + *A*_Y + *A*_Z)/3. As the trace of a hyperfine matrix is independent of its coordinate representation, the discussion of this contribution is limited to an interpretation of the *A*_{iso} values. Correlations to DFT-predicted *A*_{iso} values are depicted graphically in Fig. 3 and listed in tabular form in the Supplementary Information (Table S7). Inspection of Fig. 3 reveals that the isotropic hfcs for the various carbons, which are related to the respective electron spin density, span a wide range from −15 to about +10 MHz. Electron spin density is particularly high on the pyrazine ring system of the isoalloxazine moiety, especially at C4, C4a, C5a and C10a (with absolute *A*_{iso} values exceeding 10 MHz). Quite surprisingly, however, rather large hfcs, and hence, high spin

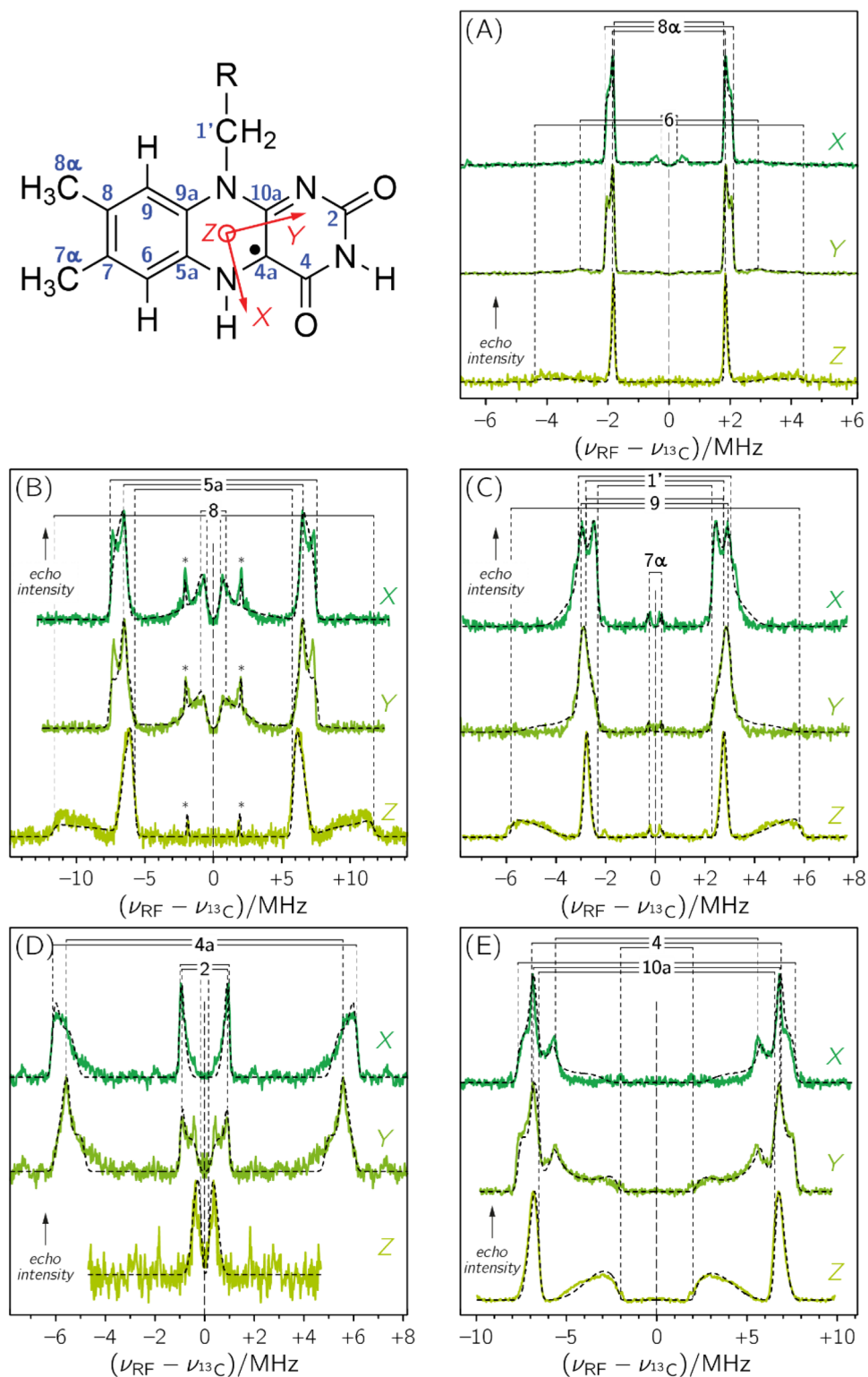


Figure 2. Frozen-solution Davies-type ENDOR spectra of specifically ^{13}C -labeled FAD cofactors in *E. coli* photolyase recorded with microwave frequencies around 94 GHz at 80 K: (A) $[6,8\alpha\text{-}^{13}\text{C}_2]$ FAD, (B) $[5\alpha,8\text{-}^{13}\text{C}_2]$ FAD (the asterisks denote resonances from the $[7,9\alpha\text{-}^{13}\text{C}_2]$ FAD isotopomer, see also Fig. S2), (C) $[1',7\alpha,9\text{-}^{13}\text{C}_3]$ FAD, (D) $[2,4\alpha\text{-}^{13}\text{C}_2]$ FAD, and (E) $[4,10\alpha\text{-}^{13}\text{C}_2]$ FAD. Spectral simulations are depicted as black dashed lines. ENDOR spectra were collected at three magnetic field positions: at g_x (dark green), g_y (medium green), and g_z (light green), see also Fig. 1.

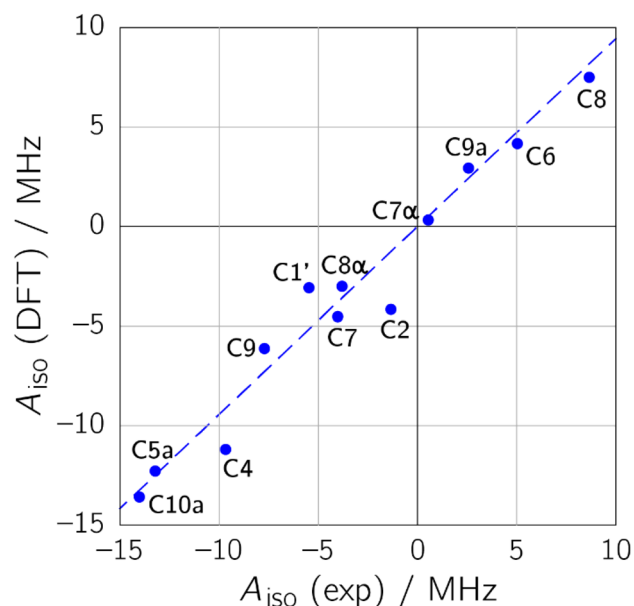


Figure 3. ENDOR/DFT correlation plot for the isotropic ^{13}C hyperfine coupling constants of the neutral FAD radical in *E. coli* photolyase. The dashed blue line represents a linear regression fit constrained to go through the origin ($R^2 = 0.9576$; slope 0.9440).

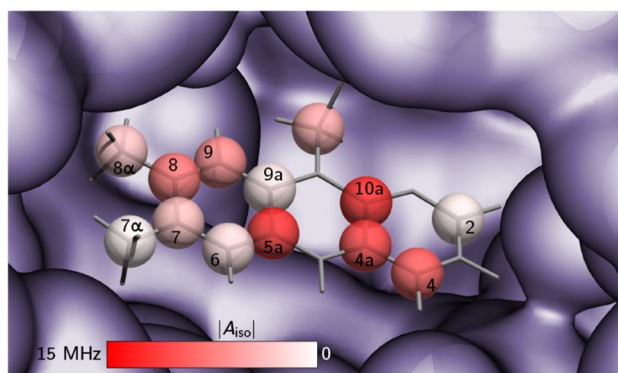


Figure 4. Flavin binding site of *E. coli* photolyase with isotropic ^{13}C hfc obtained from high-magnetic-field ENDOR hyperfine mapping (data were taken from Table S7 in the Supplementary Information). The color intensity reflects the absolute strength of a specific coupling; bright red and white colors depict strong and very weak hfc, respectively. For further details, see experimental section. Protein and cofactor geometries were taken from the PDB: 1DNP.

densities, are also observed for C1', C8 and C9. This finding could not be obtained from previous experimental spin density characterizations^{22,42,43} due to the fact that hyperfine data on H6 or H5 only inadequately probe the spin densities at C8 or C9. In contrast to that, rather low electron spin density is detected on C2, C6, C7a, C8a and C9a, which serve as probes in the pyrimidine ring and the xylene ring.

In general, experimental and calculated hfc are in good agreement, but in some cases, differences clearly exceed 15% of the absolute experimental value even though the immediate protein surroundings of the cofactor within a range of about 7 Å have been taken into account in our computations: For example, calculated hfc are far too small for position C1' and far too large for positions C2 and C4. On the other hand, there is no obvious trend of under- or overestimation between calculation and experiment, and the differences for some hfc, e.g. from C10a and C9a, are very small. We also performed more elaborate structural optimizations that did, however, not lead to a better agreement between experimental and calculated hfc, see Supplementary Information (Fig. S7 and Table S7). Nevertheless, with accurate experimental hyperfine data being now available it is henceforth possible to calibrate quantum-chemical predictions along the experiment^{44,45}.

Figure 4 illustrates the isotropic ^{13}C hfc of the isoalloxazine chromophore of FAD in *E. coli* photolyase. The characteristic distribution of the hyperfine pattern can now in principle be used to obtain an optimized electronic wavefunction of the cofactor in its paramagnetic state using quantum-chemical computations, which will then allow correlation to the specific DNA repair activity of the protein. After electron transfer from the light-excited,

fully reduced FAD cofactor to the DNA lesion (from the electron-rich pyrazine ring, presumably promoted by the adjacent adenine moiety^{46,47}), the resulting flavin-radical intermediate lives for a sufficiently long time so that cyclobutane dimer splitting can take place. Subsequently, the excess electron is pulled back to the FADH[•] intermediate, thus rendering the reaction “net-zero” with respect to a change of redox states of DNA and FAD. The driving force of this “pulling-back reaction” occurring directly from the DNA back to the FAD radical intermediate⁴⁸ is in the first place mediated by electron densities, but these need to be consistent with the experimental hyperfine structure of the radical. It is quite likely that it is enhanced by the specific electronic structure of DNA photolyases as low electron spin density on the xylene ring is assumed to increase the electron–acceptor probability of the FADH[•] intermediate. This intermediate in photolyase serves also as a model for the FADH[•] in spin-correlated radical pairs formed by photoexcitation in the related magnetoreceptor cryptochrome^{37,49}, and the hyperfine structure revealed by the present strategy will allow theoreticians to quantitatively evaluate the efficiency of magnetic sensing by taking the specific electronic structure of the radical into account^{50,51}.

In summary, the combination of high-field ENDOR with isotopologue editing establishes a basis for a more detailed understanding of the electronic characteristics of flavocoenzymes in general¹⁵. A thorough hyperfine mapping of various flavoproteins is feasible following our approach and will enable quantitative analyses of reactivity patterns of paramagnetic flavin cofactors. Such a comparison is not restricted to flavin cofactors in their ground state, but will be extended to hyperfine mapping via ENDOR spectroscopy of excited states (e.g. light-generated triplet states). With quantitative information on spin densities at hand, we have now the potential to tackle the fundamental question on the specific role of the protein surrounding on a cofactor and to assess the contributions of electronic versus steric control of a catalysed reaction.

Methods

Preparation of selectively labelled FMN. Riboflavin isotopologues were prepared as described elsewhere^{52,53}.

Preparation of DNA photolyase containing selectively labelled FAD. *E. coli* photolyase was over-expressed in *Bacillus subtilis* using a lac-controlled expression system. 5 mg/L of ¹³C-labeled riboflavin was added to vitamin-free Casamino acids medium. Protein was purified by published procedures and stored in liquid nitrogen⁵⁴.

ENDOR sample preparation. The protein concentration was estimated on the basis of the FAD cofactor’s absorbance at 580 nm ($\epsilon_{580} = 0.48 \times 10^4 \text{ M}^{-1} \text{ cm}^{-1}$). ENDOR experiments were typically performed with 1.5 mM photolyase in 0.05 M HEPES (pH 7.0) containing 0.1 M KCl and 30% (v/v) glycerol.

ENDOR instrumentation. Pulsed ENDOR spectra at 94.0 GHz were recorded using a Bruker E680 FT-EPR spectrometer described elsewhere⁵⁵. For Davies-type ENDOR spectroscopy²⁹, a $\pi/2$ pulse of 120 ns, a separation time t of 45 μs and a radio frequency pulse of 40 μs length starting 1 μs after the first microwave pulse were used. The pulse spacing was 500 ns in all experiments. All ENDOR experiments were performed at 80 K.

ENDOR data analysis. ENDOR raw data were baseline-corrected (polynomial fitting). The spectra were then normalized to a frequency of 94.0 GHz. The orientation-selective ENDOR data were analysed using global least-squares fitting to obtain the best possible agreement between experimental and calculated spectra. The Matlab-based program suite “SpecProFI”⁵⁶ [<https://www.radicals.uni-freiburg.de/de/software/specprofi>] was used to simultaneously analyse sets of three orientation-selective ENDOR spectra by using one joint set of parameters: typically two or three (depending on the specific [¹³C]FAD isotopologue) sets of hyperfine principal values ($A_{x,i}$, $A_{y,i}$ and $A_{z,i}$) and the corresponding sets of Euler angles (α_i , β_i and γ_i ; z – y – z -convention) that relate the principal axes of the respective hyperfine matrix of nucleus i to the principal axes system of the flavin’s \mathbf{g} -matrix^{31,57} (X , Y and Z ; see Fig. 1A). Weighting factors have been used to account for the specific isotope enrichment and relaxation properties of the individual ¹³C nucleus under consideration, see Supplementary Information. (The assumption of collinear hyperfine matrices and \mathbf{g} -matrix principal axes was dropped as it did not yield satisfactory spectral simulations of the experimental data.) Latin hypercube sampling^{58,59}, a powerful semi-stochastic algorithm, was invoked to increase the probability of finding the global minimum of the high-dimensional parameter hypersurface by selecting well-distributed initial parameter guesses. Subsequent optimization steps at each of these starting points were conducted by calling the “EasySpin” function “salt”, which calculates powder or single-crystal ENDOR spectra⁶⁰. In all subsequent ENDOR spectral analyses, the \mathbf{g} -matrix principal values $g_x = 2.00431$, $g_y = 2.00360$, and $g_z = 2.00217$, determined from EPR at 360 GHz/12.8 T on the neutral flavin radical in *E. coli* DNA photolyase³¹, were taken as fixed parameters.

Quantum mechanics calculations of hyperfine couplings. The input structure for the computation of hfcs was based on the crystal structure of *E. coli* photolyase³⁴. It was cut down to one layer of amino acids surrounding the FAD cofactor, which itself was truncated to riboflavin. Protons were added, and the resulting structure optimized in a semi-empirical PM3 calculation. DFT computations of hfcs were then carried out using Gaussian03⁶¹ (Gaussian Inc, Pittsburgh, PA) with the unconstrained compound functional B3LYP, the basis set EPR-II, and a tight model for the self-consistent field method. All resulting hyperfine matrices were then projected to the FADH[•]’s \mathbf{g} -matrix principal coordinate system³¹ using a self-written MATLAB-routine, see Tables S1 to S6 in the Supplementary Information. The respective hyperfine components were averaged to obtain isotropic hfcs. For Fig. 4, a self-written FORTRAN script was used to generate an input file for POV-Ray

rendering. An RGB colour value was calculated corresponding to $|A_{\text{iso}}|$, with the largest value representing RGB 1–0–0 (red) and the smallest RGB 1–1–1 (white).

Received: 15 April 2021; Accepted: 24 August 2021

Published online: 14 September 2021

References

- Theorell, H. Quantitative Bestrahlungsversuche an gelbem Ferment, Flavinphosphorsäure und Lactoflavin. *Biochem. Z.* **279**, 186–200 (1935).
- Massey, V. Introduction: Flavoprotein structure and mechanism. *FASEB J.* **9**, 473–475 (1995).
- Massey, V. The chemical and biological versatility of riboflavin. *Biochem. Soc. Trans.* **28**, 283–296 (2000).
- Saraste, M. Oxidative phosphorylation at the fin de siècle. *Science* **283**, 1488–1493 (1999).
- Fraaije, M. W. & Mattevi, A. Flavoenzymes: Diverse catalysts with recurrent features. *Trends Biochem. Sci.* **25**, 126–132 (2000).
- Heuts, D. P. H. M., Scrutton, N., McIntire, W. S. & Fraaije, M. W. What's in a covalent bond? On the role and formation of covalently bound flavin cofactors. *FEBS J.* **276**, 3405–3427 (2009).
- Bornemann, S. Flavoenzymes that catalyse reactions with no net redox change. *Nat. Prod. Rep.* **19**, 761–772 (2002).
- Sancar, A. Structure and function of DNA photolyase and cryptochrome blue-light photoreceptors. *Chem. Rev.* **103**, 2203–2237 (2003).
- Weber, S. Light-driven enzymatic catalysis of DNA repair: A review of recent biophysical studies on photolyase. *Biochim. Biophys. Acta* **1707**, 1–23 (2005).
- van der Horst, M. A. & Hellingwerf, K. J. Photoreceptor proteins, “Star Actors of Modern Times”: A review of the functional dynamics in the structure of representative members of six different photoreceptor families. *Acc. Chem. Res.* **37**, 13–20 (2004).
- Müller, M. & Carell, T. Structural biology of DNA photolyases and cryptochromes. *Curr. Opin. Struct. Biol.* **19**, 277–285 (2009).
- Zhang, M., Wang, L. & Zhong, D. Photolyase: Dynamics and electron-transfer mechanisms of DNA repair. *Arch. Biochem. Biophys.* **632**, 158–174 (2017).
- Bouly, J.-P. *et al.* Cryptochrome blue-light photoreceptors are activated through interconversion of flavin redox states. *J. Biol. Chem.* **282**, 9383–9391 (2007).
- Kay, C. W. M. *et al.* Blue light perception in plants. Detection and characterization of a light-induced neutral flavin radical in a C450A mutant of phototropin. *J. Biol. Chem.* **278**, 10973–10982 (2003).
- Kar, R. K., Miller, A.-F. & Mroginiski, M.-A. Understanding flavin electronic structure and spectra. *Wiley Interdiscip. Rev. Comput. Mol. Sci.* **2021**, e1541 (2021).
- Ghisla, S. & Massey, V. New flavins for old: Artificial flavins as active site probes of flavoproteins. *Biochem. J.* **239**, 1–12 (1986).
- Bacher, A., Illarionov, B., Eisenreich, W. & Fischer, M. Ch. 4. In *Flavins and Flavoproteins. Methods and Protocols Methods in Molecular Biology Springer Protocols* (eds Weber, S. & Schleicher, E.) 65–78 (Springer, 2014).
- Iorgu, A. I., Cliff, M. J., Waltho, J. P., Scrutton, N. S. & Hay, S. Isotopically labeled flavoenzymes and their uses in probing reaction mechanisms. *Methods Enzymol.* **620**, 145–166 (2019).
- Bennati, M. EPR interactions—Hyperfine couplings. *eMagRes* **6**, 271–282 (2017).
- Kay, C. W. M. *et al.* EPR, ENDOR and TRIPLE resonance spectroscopy on the neutral flavin radical in *Escherichia coli* DNA photolyase. *Biochemistry* **38**, 16740–16748 (1999).
- Barquera, B. *et al.* X- and W-band EPR and Q-band ENDOR studies of the flavin radical in the Na⁺-translocating NADH:Quinone oxidoreductase from *Vibrio cholerae*. *J. Am. Chem. Soc.* **125**, 265–275 (2003).
- Brosi, R. *et al.* Coupled methyl group rotation in FMN radicals revealed by selective deuterium labeling. *J. Phys. Chem. B* **124**, 1678–1690 (2020).
- Brosi, R. *et al.* Hindered rotation of a cofactor methyl group as a probe for protein–cofactor interaction. *J. Am. Chem. Soc.* **132**, 8935–8944 (2010).
- Schleicher, E. *et al.* The electronic state of flavoproteins: Investigations with proton electron–nuclear double resonance. *Appl. Magn. Reson.* **37**, 339–352 (2010).
- Bennati, M. *et al.* Pulsed electron–nuclear double resonance (ENDOR) at 140 GHz. *J. Magn. Reson.* **138**, 232–243 (1999).
- Epel, B., Niklas, J., Sinnecker, S., Zimmermann, H. & Lubitz, W. Phylloquinone and related radical anions studied by pulse electron nuclear double resonance spectroscopy at 34 GHz and density functional theory. *J. Phys. Chem. B* **110**, 11549–11560 (2006).
- Goldfarb, D. High field ENDOR as a characterization tool for functional sites in microporous materials. *Phys. Chem. Chem. Phys.* **8**, 2325–2343 (2006).
- Möbius, K., Lubitz, W., Cox, N. & Savitsky, A. Biomolecular EPR meets NMR at high magnetic fields. *Magnetochemistry* **4**, Art. No. 50 (2018).
- Harmer, J. R. Hyperfine spectroscopy—ENDOR. *eMagRes* **5**, 1493–1514 (2016).
- Schnegg, A. Very-high-frequency EPR. *eMagRes* **6**, 115–132 (2017).
- Fuchs, M. *et al.* The g-tensor of the neutral flavin radical cofactor of DNA photolyase revealed by 360-GHz electron paramagnetic resonance spectroscopy. *J. Phys. Chem. B* **106**, 8885–8890 (2002).
- Schnegg, A. *et al.* The g-tensor of the flavin cofactor in (6–4) photolyase: A 360 GHz/12.8 T electron paramagnetic resonance study. *Mol. Phys.* **104**, 1627–1633 (2006).
- Sancar, A. No, “End of History” for photolyases. *Science* **272**, 48–49 (1996).
- Park, H.-W., Kim, S.-T., Sancar, A. & Deisenhofer, J. Crystal structure of DNA photolyase from *Escherichia coli*. *Science* **268**, 1866–1872 (1995).
- Mees, A. *et al.* Crystal structure of a photolyase bound to a CPD-like DNA lesion after in situ repair. *Science* **306**, 1789–1793 (2004).
- Rodgers, C. T. & Hore, P. J. Chemical magnetoreception in birds: The radical pair mechanism. *Proc. Natl. Acad. Sci. USA* **106**, 353–360 (2009).
- Biskup, T. *et al.* Direct observation of a photoinduced radical pair in a cryptochrome blue-light photoreceptor. *Angew. Chem. Int. Ed.* **48**, 404–407 (2009).
- James, C. D., Wiley, S., Ragsdale, S. W. & Hoffman, B. M. ¹³C electron nuclear double resonance spectroscopy shows acetyl-CoA synthase binds two substrate CO in multiple binding modes and reveals the importance of a CO-binding “alcove”. *J. Am. Chem. Soc.* **142**, 15362–15370 (2020).
- Stoll, S. Pulse EPR. *eMagRes* **6**, 23–38 (2017).
- Weber, S., Möbius, K., Richter, G. & Kay, C. W. M. The electronic structure of the flavin cofactor in DNA photolyase. *J. Am. Chem. Soc.* **123**, 3790–3798 (2001).
- García, J. I. *et al.* Theoretical analysis of the electron spin density distribution of the flavin semiquinone isoalloxazine ring within model protein environments. *J. Phys. Chem. A* **106**, 4729–4735 (2002).

42. Medina, M. & Cammack, R. ENDOR and related EMR methods applied to flavoprotein radicals. *Appl. Magn. Reson.* **31**, 457–470 (2007).
43. Martínez, J. I., Alonso, P. J. & Medina, M. The electronic structure of the neutral isoalloxazine semiquinone within *Anabaena* flavodoxin: New insights from HYSCORE experiments. *J. Magn. Reson.* **218**, 153–162 (2012).
44. Kirste, B. DFT calculations of hyperfine coupling constants of organic π radicals and comparison with empirical equations and experiment. *Magn. Reson. Chem.* **54**, 835–841 (2016).
45. Witwicki, M., Walencik, P. K. & Jezierska, J. How accurate is density functional theory in predicting spin density? An insight from the prediction of hyperfine coupling constants. *J. Mol. Model.* **26**, 10 (2020).
46. Antony, J., Medvedev, D. M. & Stuchebrukhov, A. A. Theoretical study of electron transfer between the photolyase catalytic cofactor FADH⁺ and DNA thymine dimer. *J. Am. Chem. Soc.* **122**, 1057–1065 (2000).
47. Acocella, A., Jones, G. A. & Zerbetto, F. What is adenine doing in photolyase?. *J. Phys. Chem. B* **114**, 4101–4106 (2010).
48. Kao, Y.-T., Saxena, C., Wang, L., Sancar, A. & Zhong, D. Direct observation of thymine dimer repair in DNA by photolyase. *Proc. Natl. Acad. Sci. USA* **102**, 16128–16132 (2005).
49. Hochstoeger, T. *et al.* The biophysical, molecular, and anatomical landscape of pigeon CRY4: A candidate light-based quantal magnetoreceptor. *Sci. Adv.* **6**, eabb9110 (2020).
50. Zhang, Y., Berman, G. P. & Kais, S. The radical pair mechanism and the avian chemical compass: Quantum coherence and entanglement. *Int. J. Quantum Chem.* **115**, 1327–1341 (2015).
51. Hore, P. J. & Mouritsen, H. The radical-pair mechanism of magnetoreception. *Annu. Rev. Biophys.* **45**, 299–344 (2016).
52. Sedlmaier, H., Müller, F., Keller, P. J. & Bacher, A. Enzymatic-synthesis of riboflavin and FMN specifically labeled with ¹³C in the xylene ring. *Z. Naturforsch. C* **42**, 425–429 (1987).
53. Römisch, W., Eisenreich, W., Richter, G. & Bacher, A. Rapid one-pot synthesis of riboflavin isotopomers. *J. Org. Chem.* **67**, 8890–8894 (2002).
54. Schleicher, E. *et al.* Light-induced reactions of *Escherichia coli* DNA photolyase monitored by Fourier transform infrared spectroscopy. *FEBS J.* **272**, 1855–1866 (2005).
55. Kay, C. W. M. *et al.* Determination of the g-matrix orientation in flavin radicals by high-field/high-frequency electron-nuclear double resonance. *Magn. Reson. Chem.* **43**, S96–S102 (2005).
56. Rein, S., Quintes, F., Quintes, T., Kacprzak, S. & Weber, S. SpecProFi: An open-source Matlab-based data processing and fitting framework to globally analyze multiple EPR data sets. (2021).
57. Weber, S., Kay, C. W. M., Bacher, A., Richter, G. & Bittl, R. Probing the N(5)–H bond of the isoalloxazine moiety of flavin radicals by X- and W-band pulsed electron–nuclear double resonance. *ChemPhysChem* **6**, 292–299 (2005).
58. McKay, M. D., Beckman, R. J. & Conover, W. J. A comparison of three methods for selecting values of input variables in the analysis of output from a computer code. *Technometrics* **21**, 239–245 (1979).
59. Iman, R. L., Helton, J. C. & Campbell, J. E. An approach to sensitivity analysis of computer models: Part I. Introduction, input variable selection and preliminary variable assessment. *J. Qual. Technol.* **13**, 174–183 (1981).
60. Stoll, S. & Schweiger, A. EasySpin, a comprehensive software package for spectral simulation and analysis in EPR. *J. Magn. Reson.* **178**, 42–55 (2006).
61. Frisch, M. J. *et al.* Gaussian 03 (Revision B.04). (2003).

Acknowledgements

This work was supported by the Deutsche Forschungsgemeinschaft (DFG; Projects WE2376/4-1, WE2376/4-2, FI 824/6-1). We thank Dr. Bernd Paulus for preparing Fig. 4. The DFT and QM/MM calculations presented in the Supporting Information have been performed on a large-capacity computer in the bw|HPC center within Grant bw15A007.

Author contributions

E.S., R.B., A.B., M.F. and S.W. designed the research and conceived the experiments. The sample preparation was performed by B.I. E.S. conducted the pulsed EPR and ENDOR experiments. E.S., S.R. and S.W. analysed and interpreted the ENDOR data. A.L. and S.K. performed QM/MM calculations, and S.W., T.A.S. and S.K. DFT computations of anisotropic hyperfine couplings. The figures were created by S.W., S.R. and E.S. The manuscript was written through contributions of all authors. All authors have reviewed the manuscript.

Funding

Open Access funding enabled and organized by Projekt DEAL.

Competing interests

The authors declare no competing interests.

Additional information

Supplementary Information The online version contains supplementary material available at <https://doi.org/10.1038/s41598-021-97588-7>.

Correspondence and requests for materials should be addressed to E.S. or S.W.

Reprints and permissions information is available at www.nature.com/reprints.

Publisher's note Springer Nature remains neutral with regard to jurisdictional claims in published maps and institutional affiliations.



Open Access This article is licensed under a Creative Commons Attribution 4.0 International License, which permits use, sharing, adaptation, distribution and reproduction in any medium or format, as long as you give appropriate credit to the original author(s) and the source, provide a link to the Creative Commons licence, and indicate if changes were made. The images or other third party material in this article are included in the article's Creative Commons licence, unless indicated otherwise in a credit line to the material. If material is not included in the article's Creative Commons licence and your intended use is not permitted by statutory regulation or exceeds the permitted use, you will need to obtain permission directly from the copyright holder. To view a copy of this licence, visit <http://creativecommons.org/licenses/by/4.0/>.

© The Author(s) 2021